AGU PUBLICATIONS

JGR

Journal of Geophysical Research: Planets

RESEARCH ARTICLE
10.1002/2013JE004519

Special Section:
Results from the first 360 Sols of the Mars Science Laboratory Mission: Bradbury Landing through Yellowknife Bay

Key Points:
- APXS response for samples on the MSL Ti science observation tray is investigated
- Results from MSL-APXS measurement of scooped Rocknest drift sample are presented
- Techniques for modeling and evaluating APXS-thin samples are presented

Correspondence to:
J. A. Berger,
jberge44@uwo.ca

Citation:
Berger, J. A., et al. (2014), MSL-APXS titanium observation tray measurements: Laboratory experiments and results for the Rocknest fines at the *Curiosity* field site in Gale Crater, Mars, *J. Geophys. Res. Planets*, *119*, 1046–1060, doi:10.1002/2013JE004519.

Received 2 SEP 2013
Accepted 6 APR 2014
Accepted article online 23 APR 2014
Published online 13 MAY 2014

MSL-APXS titanium observation tray measurements: Laboratory experiments and results for the Rocknest fines at the *Curiosity* field site in Gale Crater, Mars

Jeff A. Berger[1], Penelope L. King[2,3], Ralf Gellert[3], J. L. Campbell[3], Nicholas I. Boyd[3], Irina Pradler[3], Glynis M. Perrett[3], Kenneth S. Edgett[4], Scott J. V. VanBommel[3], Mariek E. Schmidt[5], and Rebekka E. H. Lee[5]

[1]Department of Earth Sciences, University of Western Ontario, London, Ontario, Canada, [2]Research School of Earth Sciences, Australian National University, Canberra, ACT, Australia, [3]Guelph-Waterloo Physics Institute, University of Guelph, Guelph, Ontario, Canada, [4]Malin Space Science Systems, San Diego, California, USA, [5]Department of Earth Sciences, Brock University, St. Catharines, Ontario, Canada

Abstract The Mars Science Laboratory (MSL) rover, *Curiosity*, has a titanium science observation tray (o-tray), upon which portions from drilled and scooped Martian samples can be delivered for analyses by the Alpha-Particle X-ray Spectrometer (APXS). The standard APXS calibration approach to derive elemental concentrations cannot be applied to samples on the o-tray because they (1) have a nonuniform three-dimensional distribution within the APXS field of view and (2) are thin (< 50 μm) compared to the APXS information depth for heavy elements (> 90 μm). To develop techniques for interpreting MSL-APXS o-tray measurements, we conducted laboratory measurements of thin particulate basalt samples on Ti metal with the Flight Equivalent APXS Unit. The experiments demonstrate that, relative to an "infinitely thick" sample, increasing areal coverage of particulates on a Ti metal substrate results in a proportional decrease in the Ti signal and increase in the sample signal. Count rates for heavier elements (Mn and Fe) drop with decreasing sample thickness because the mean thickness is smaller than the APXS information depth. Similar effects were seen in the MSL-APXS o-tray measurement of Rocknest fines on Martian solar day 95, an aliquot of material delivered to Sample Analysis at Mars and Chemistry and Mineralogy. The thin layer effect caused a drop in Mn and Fe signals, which cannot be quantitatively compared to the in situ Rocknest target "Portage" because sample thickness was unknown. Otherwise, Rocknest fines on the o-tray had no significant compositional differences from Portage, except for slight increases in S and Cl.

1. Introduction

A titanium science observation tray (o-tray) is mounted on the front of the Mars Science Laboratory (MSL) rover, *Curiosity* [*Anderson et al.*, 2012], upon which portions from drilled and scooped Martian samples can be delivered for analyses by rover cameras and the Alpha-Particle X-ray Spectrometer (APXS) [*Gellert et al.*, 2006, 2009; *Campbell et al.*, 2012]. The o-tray is an important tool to assess physical fractionation and chemical changes in samples after collection and processing by the sampling subsystem on the rover arm. These high-value samples, portions of which are delivered to *Curiosity's* science instruments SAM (Sample Analysis at Mars) [*Mahaffy et al.*, 2012] and CheMin (Chemistry and Mineralogy) [*Blake et al.*, 2012], are usually investigated thoroughly in situ before being scooped or drilled. Sample collection and processing by MSL's Sample Acquisition, Processing, and Handling (SA/SPaH) Collection and Handling for Interior Martian Rock Analysis (CHIMRA) subsystem [*Anderson et al.*, 2012] involves multiple pathways from the drill or scoop, moving through the system via a series of arm movements and facilitated by a vibrating mechanism. Sample material, sieved through 150 μm or 1 mm screens, is stored in reservoirs before it is ultimately delivered to SAM and/or CheMin. An aliquot from the < 150 μm reservoir (or < 1 mm from the scoop) can be deposited on the o-tray for investigation by APXS, MAHLI (Mars Hand Lens Imager) [*Edgett et al.*, 2012], and Mastcam [*Bell et al.*, 2012]. This enables characterization of the processed sample, which may have a different composition than the in situ sample. Using APXS to determine the chemical composition of portions of the same material as delivered to SAM and CheMin is crucial for interpreting MSL data, and is the best practice in utilizing the MSL instrument suite.

The o-tray is a flat, circular tray 7.5 cm in diameter that was constructed of commercially pure titanium metal [*Anderson et al.*, 2012] because Ti has the lowest response for APXS [*Omand et al.*, 2005; *Gellert et al.*, 2006;

Brückner et al., 2008]. Materials invisible to APXS, such as Teflon, could not be used because they are nonconductive and the buildup of charge could cause adherence and other unwanted behavior of deposited samples or environmental dust. In most sample dropoff scenarios, the Ti substrate precludes the assessment of Ti in the sample, but it enables use of the absorption of the Ti o-tray signal in the overlying sample to provide an estimate of the total sample amount.

The relatively small volume of sample material portioned to the o-tray (~75 mm^3 per portion) [*Anderson et al*., 2012] poses challenges for the APXS technique. In typical APXS measurements of rocks and regolith fines, the samples can always be assumed infinitely thick and yields for the elemental signals can be calculated in the sample. The effective APXS "information depth" is dependent on the degree to which excited characteristic X-rays are attenuated as they travel through the specimen. This attenuation depends upon the X-ray energy and hence on the element concerned, and the transmitted fraction falls exponentially with distance; it follows that there is not a well-defined "range." A widely used definition of the information depth is the depth within which 90% of the detected X-rays have been generated. Elements with a low atomic number (Z) have a smaller information depth (normally < 10 μm) than high Z elements [*Rieder et al*., 2003; *Brückner et al*., 2008; *Campbell et al*., 2009]. The overall sample matrix composition largely determines the information depth. Within a basalt matrix, for example, 90% of the Fe X-rays are excited from a volume with a depth of 89 μm, while the same yield for Si X-rays occurs from a volume with a depth of 6 μm [*Campbell et al*., 2009]. Small samples on the o-tray are unlikely to be "infinitely thick" with respect to the information depth, and the decreased volume from which X-rays are excited yields a lower signal than an infinitely thick sample. The actual abundances of elements are thus not measured directly. Additionally, the three-dimensional distribution (thickness and area coverage) of sample on the o-tray is not uniform; the sample only partially covers the APXS field of view (FOV) with spatially variable thickness. Since the detailed depth distribution of the sample is unknown, correcting for the thin layer effect comes with large uncertainty. This is a particular concern for Fe, a major element in most Martian materials. A further consideration with thin samples is the flux of Ti X-rays from the o-tray, which can excite very efficiently X-rays from Ca, K, and Cl, skewing their apparent concentrations to higher levels by up to 10%.

Uncertainty and variability in environmental conditions and in sample properties make depositing the sample on the o-tray in an accurate, reproducible fashion nearly impossible. Portions dropped from CHIMRA may not ideally cover the full APXS FOV, which varies with standoff distance (FOV increases from ~1.7 cm to ~3.1 cm as standoff distance increases from 1.8 cm to 3.8 cm from the detector). Exposed o-tray in the FOV results in a prominent Ti peak and elevated background (shelf) at lower energy (< 5 keV) stemming from incomplete charge collection of the Ti peak in the detector [e.g., *Gellert et al*., 2006]. Dropping the sample from CHIMRA also results in a rough, uneven surface that introduces uncertainty to APXS interpretations [*Campbell and Cookson*, 1984; *Campbell et al*., 1985].

The two main objectives of this study are to (1) develop a practical method for interpreting MSL-APXS measurements of samples on the o-tray and (2) present and interpret results from the MSL-APXS measurement of fines scooped, processed, and delivered to the o-tray at the Rocknest sampling site in October and November 2012. To assess the o-tray challenges discussed above, we conducted laboratory experiments with the Flight Equivalent APXS Unit (FEU-APXS). Spectrum fitting and X-ray yield modeling software were used to understand these data. Complex factors that affect APXS operations on Mars, such as sample heterogeneity, sample/detector geometry, and roughness, have been discussed elsewhere [e.g., *Rieder et al*., 2003; *Gellert et al*., 2006; *Brückner et al*., 2008; *Foley et al*., 2008; *Campbell et al*., 2010, 2011b, 2012], and here we focus on unique conditions for the MSL o-tray.

2. Treatment of APXS Spectra

Element peak areas were derived from APXS spectra using a spectrum fitting code, GUAPX, which was developed for APXS [*Campbell et al*., 2011a, 2011b, 2012]. The code handles particle-induced X-ray emission (PIXE) and X-ray fluorescence (XRF) analyses simultaneously, which is the basis of the APXS technique. Samples were treated as unknowns, requiring an iterative fitting method. For infinitely thick samples, iterations converge on the model spectrum according to the closure rule, first converting peak areas to element concentrations and then to oxide concentrations, normalizing such that oxides sum to 100%. Titanium was assumed to be uncoupled with oxygen because its signal was dominated by the Ti metal substrate. The program allows empirical corrections based on sample type (e.g., basalt and andesite); these were not applied in this work. Error for all spectrum fitting in this work is reported as 2σ fit error, compounded in ratios where appropriate.

Table 1. LA ICP-MS Results for Ti Metal

	Mg	Al	Si	P	S	V	Cr	Mn	Fe	Co	Ni	Zn	Ge	Zr	Sn	Ta
Mass measured	25	27	29	31	34	51	52	55	57	59	61	68	72	91	118	181
Mean (ppm)	166	79	2210	43	1084	2	103	3	1585	1	90	6	0.1	4	12	0.5
1δ (ppm)	23	9	236	18	68	0.2	32	1	1881	1	48	3	0.5	0.4	0.4	0.05
Spikes[a]				√			√		√	√	√					

[a]Intermittent peaks due to microscale variation (see text).

In some cases, it was necessary to compare element peak areas for samples measured at different standoff distances, requiring a correction for the drop in signal with distance. We calculated geometric normalization factors using empirical curves derived from APXS measurements at different standoff distances. One curve was determined for the FEU-APXS using calibration data from *Campbell et al*. [2012], and another was determined for the MSL-APXS using data acquired at the Gale Crater site over Martian solar days (= 24.6 h) (sols) 0–330. Uncertainty was estimated from the variance in the data (absolute error of 1% for FEU and 5% for MSL) and is added to the ratios reported below.

3. FEU-APXS Ti-Tray Experiments

The experiments described below test the APXS response to a geologic sample on a Ti metal substrate. We used the same Ti metal as used for the o-tray on *Curiosity*, provided by the Jet Propulsion Laboratory. For this work, we define "o-tray samples" as samples measured by MSL-APXS on the titanium science observation tray on *Curiosity* and "Ti-tray samples" as samples prepared for analysis with the FEU-APXS using pieces of Ti metal.

3.1. Ti-Tray Methodology

To simulate a small geologic sample on Ti in a controlled manner, particulates of Broken Tank (BT2) basalt were dusted uniformly over pieces of Ti metal and measured with the FEU-APXS. BT2 was selected because it is (1) of mafic composition similar to Martian materials and (2) used for the APXS calibration target on *Curiosity* and is well characterized for APXS [*Burkemper et al*., 2008; *King et al*., 2010; *Campbell et al*., 2013; *Thompson et al*., 2013]. BT2 is an alkali basalt with an ophitic to subophitic texture composed primarily of ~500 μm grain size Ca- and Na-bearing plagioclase feldspar, augite, alkali feldspar, and olivine with minor oxides (ilmenite, Fe-Ti spinel, and chromite) and apatite [*Thompson et al*., 2013]. Minor alteration associated with olivine is present in veins and halos as clays, chlorite, possible biotite, and hydrated iron oxides [*Thompson et al*., 2013]. The sample material was homogeneous and fine-grained, with no large crystals or inclusions. An aliquot of approximately 10 g weight taken from a large sample (~10 kg) of walnut/pea sized, washed BT2 basalt was crushed in a steel mill and sieved to < 150 μm to obtain a particulate size range comparable to the < 150 μm samples prepared by CHIMRA. An aliquot of this particulate was prepared as a smooth, flat, and APXS-thick (> 2 mm) bulk sample held in an Al dish with the method described by *Campbell et al*. [2012]. The Ti metal was cut to 2.5 cm × 2.5 cm pieces using an electrical discharge machine, cleaned with phosphoric acid, and mounted in an Al dish. The Ti-tray samples were prepared by dusting the BT2 particulates uniformly over the Ti surface through a 250 μm sieve. Several different BT2 masses were deposited to achieve a range of areal coverage and thickness. Micrographs documented the surfaces for calculation of percent areal coverage of the particulate with image software. No adhesive was used to preserve the surface; the Ti-tray samples were prepared and documented immediately before placement in the FEU-APXS vacuum chamber, where a visual inspection was made to confirm that the particulate was not disturbed.

Additional particulate separates were made from the BT2 < 150 μm bulk sample to investigate the effects of sieving on phase fractionation, potentially causing variation in elemental X-ray yield. Two particulates were prepared by sieving to 125–150 μm and to < 32 μm. One sample was prepared using a different method to achieve a film of BT2: < 150 μm BT2 was placed on the Ti surface, which was then inverted to remove most of the material, leaving behind a film. The film was too fine to characterize with an optical microscope.

We determined the composition of a piece of the Ti metal that was cut from the same material used for both the MSL o-tray and the Ti-tray laboratory experiments. The Ti was inspected with scanning electron microscopy for impurities, but none were noted. To examine homogeneity on small scale, a 20 point line scan of 30 μm spots was conducted using laser ablation inductively coupled plasma-mass spectrometry (LA ICP-MS) at the Australian National University. The system is an Agilent 7700 with a COMPex 110 excimer laser beam that was

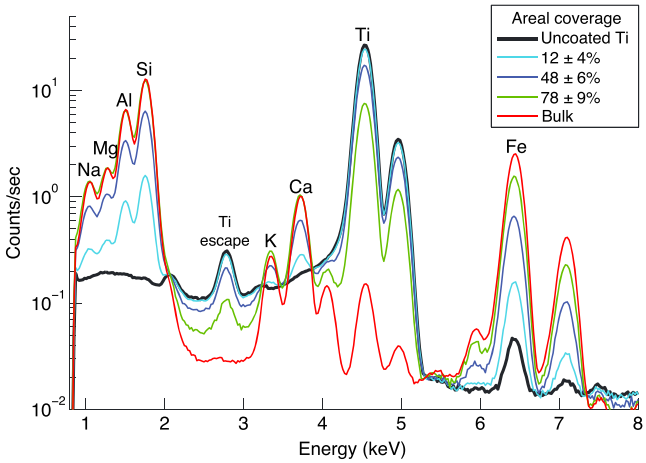

Figure 1. FEU-APXS spectra of BT2 < 150 μm particulates on Ti substrates, with the uncoated Ti metal and bulk BT2. Relative to the uncoated Ti, increasing the areal coverage and thickness of BT2 particulates decreases the Ti signal and increases the sample signal. Select Kα peaks and the Ti Kα escape peak are labeled.

operated at 5 Hz and 50 mJ. A custom-made HelEx cell was used to contain the samples. We used peak hopping mode to analyze the isotopes and an integration time of 0.01 s for all elements. We followed a sequence of 35 s with the laser on and 35 s for the gas background. Counts were averaged over 25 s interval at maximum peak intensity.

The Ti-tray samples were analyzed in the Guelph APXS calibration setup using the FEU-APXS instruments [*Gellert et al.*, 2006; *Campbell et al.*, 2012]. Measurements were done in nominal vacuum (~ 0.2 mbar) with the aluminum dish in the standard position.

3.2. Ti-Tray Results

Results from LA ICP-MS show that the Ti metal contains minor amounts of impurities (Table 1). All elements are below ~0.2 wt %, with the highest concentrations for Si (2210 ± 236 ppm), Fe (1585 ± 1881 ppm), and S (1084 ± 68 ppm). The Ti metal is not homogeneous on the microscale in terms of Fe, Cr, Co, and P, (and perhaps Ni, Zn, and Mn), as seen in intermittent spectral peaks for those elements recorded during depth profiling. These variations are interpreted as Fe and Fe-Cr-P-Co and inclusions that contribute to the large variation between individual LA ICP-MS small-scale analyses. This variation is further considered to be related to microscale variations in the sample, not the error of the technique, because the BCR-2G standard that was measured at the same time agreed with GeoReM preferred values for all elements except Zn and Ge that are different due to interferences. However, the Zn and Ge contents of the Ti metal are very low, therefore, those interferences are not critical. Comparing Table 1 with the typical concentrations expected in Martian materials, only S, Cr, Ni, and possibly Si and Fe at lower areal coverage might make significant contributions to the peak areas that require corrections.

The FEU-APXS spectrum of the Ti metal is dominated by Ti Kα and Kβ peaks, with an associated background (shelf) over the spectrum < 5 keV (Figure 1). A Ti escape peak is apparent at ~2.77 keV. Element concentrations were derived with GUAPX assuming no surface oxidation, with all elements uncoupled with oxygen in the calculations. The only impurities with confirmed peaks are Fe at 0.24 cts/s ± 4.1% and Ni at 0.03 cts/s ± 23.5% (Table 3).

APXS spectra of the Ti-tray samples (Table 2) demonstrate that increasing the fractional area coverage and thickness of < 150 μm BT2 particulates decreases the Ti signal and increases the BT2 sample signal (Figure 1). Differences in the spectra are illustrated by the elemental ratios of Ti-tray samples (BT2 + Ti substrate) to the

Table 2. FEU-APXS Ti-Tray Sample Summary

Sample	Particulate Size (μm)	Particulate Mass (mg)	Areal Coverage (%)	Mass/Area (mg/cm^2)	Integration Time (s)	FWHM Mn (eV)[a]
TI_0	N/A	None	0	0	66,730	195.0
BT2JFR	< 150	Bulk	N/A	N/A	79,208	189.6
Ti_BT2_150_75	< 150	47 ± 1	78 ± 9	7.5 ± 0.9	15,001	194.7
Ti_BT2_150_50	< 150	13 ± 1	48 ± 6	2.1 ± 0.3	24,003	198.8
Ti_BT2_150_15	< 150	3 ± 1	12 ± 4	0.5 ± 0.5	44,404	196.5
Ti_BT2_125_50	125–150	46 ± 1	55 ± 5	7.4 ± 0.6	76,211	191.9
Ti_BT2_32_50	< 32	3 ± 1	28 ± 4	0.5 ± 0.1	56,407	193.5
Ti_BT2_film	Unk	0.176 ± 0.035	Film	N/A	76,807	193.6

[a]FWHM, Full width at half maximum.

Table 3. FEU-APXS Peak Areas of the BT2 Ti-Tray Samples[a]

Sample Mass/area (mg/cm^2)	Ti_0 Ti Metal N/A		BT2JFR Bulk BT2 N/A		Ti_BT2_150_75 7.5 ± 0.9		Ti_BT2_150_50 2.1 ± 0.3		Ti_BT2_150_15 0.5 ± 0.5		Ti_BT2_125_50 7.4 ± 0.6		Ti_BT2_32_50 0.5 ± 0.1		Ti_BT2_film N/A	
% Areal coverage	78 ± 9		78 ± 9		48 ± 6		12 ± 4		55 ± 5		28 ± 4		Unk			
	Area (cts/s)	%Fit Error	Area (cts/s)	%Fit Error	Area (cts/s)	%Fit Error	Area (cts/s)	%Fit Error	Area (cts/s)	%Fit Error	Area (cts/s)	%Fit Error	Area (cts/s)	%Fit Error	Area (cts/s)	%Fit Error
Na	nd		7.17	3.2	5.20	5.0	2.78	6.0	0.63	11.0	3.32	4.2	1.48	6.3	0.27	17.3
Mg	nd		10.7	3.7	7.53	5.7	4.12	6.6	0.93	10.7	4.65	4.8	2.86	5.4	0.43	14.8
Al	nd		44.1	2.0	34.1	2.5	17.8	2.8	4.05	3.7	21.9	2.2	9.79	2.7	2.04	4.2
Si	nd		90.3	1.2	71.6	1.4	37.1	1.6	8.70	2.0	44.4	1.3	21.8	1.6	3.05	2.8
K	nd		1.85	2.2	1.50	3.8	0.76	6.0	0.15	20.2	0.87	3.7	0.42	7.4	nd	
Ca	nd		7.70	1.5	6.21	2.2	3.12	2.8	0.79	5.8	3.98	2.0	1.91	3.0	0.23	14.7
Ti	178.6	0.9	1.15	2.3	51.7	1.1	118.5	1.0	165.5	0.9	97.9	0.9	145.8	1.0	177.0	1.0
Mn	nd		0.20	7.5	0.13	15.3	0.05	26.9	nd		0.08	11.7	0.03	28.2	nd	
Fe	0.24	4.1	22.6	1.0	11.0	1.3	4.72	1.5	1.06	2.1	7.43	1.1	2.42	1.5	0.30	3.4
Ni	0.03	23.5	0.05	13.2	0.04	30.4	0.02	37.4	0.02	33.5	0.03	17.8	0.02	28.4	nd	
Zn	nd		0.06	10.6	0.02	51.8	nd		nd		0.01	42.3	nd		nd	

[a]Peak areas are scaled to represent the same standard geometry with geometric normalization = 1. The geometric normalization factor of BT2JFR is 1.00; for all other Ti-tray samples the geometric normalization is 1.26 ± 0.01. nd = not detected.

bulk BT2, using peak area in counts/second (Table 3; Figure 2a). Due to differences in the machining of the sample mounts, the Ti-tray samples were 4.25 mm closer to the detector than the bulk BT2. To correct for this, a geometric normalization factor of 1.26 ± 0.01 was applied to the bulk BT2 peak areas. This factor was derived empirically from distance measurements of basalt, andesite, and anorthosite geologic reference materials, and corresponds with previous studies of APXS standoff [*Gellert et al.*, 2006]. The peak area ratios for elements with energies less than 4 keV are proportional to the areal coverage of the sample.

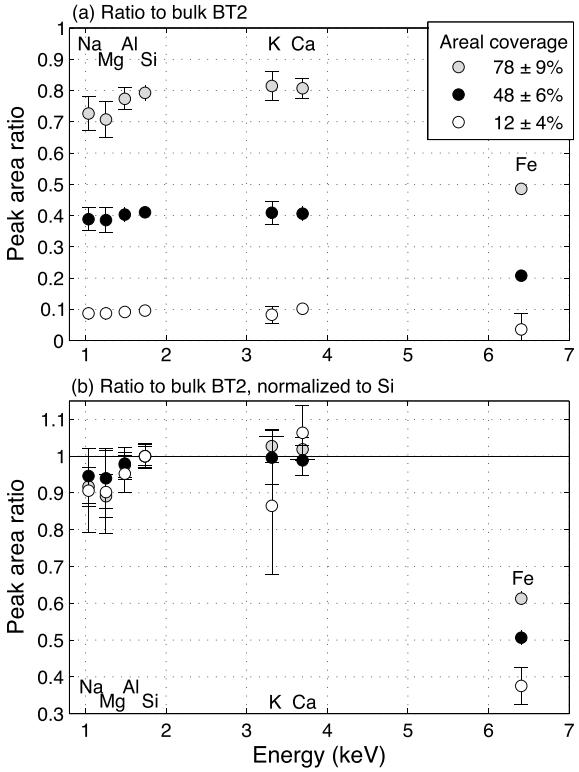

Figure 2. (a) Peak area ratios of < 150 μm Ti-tray samples (BT2 + Ti substrate) to bulk BT2. The peak area ratios are proportional to the areal coverage of the sample. Iron is lower than lighter elements, indicating that the mean thickness is smaller than the Fe sampling depth. (b) The peak area ratios are normalized to Si, showing the drop in signal for Fe is greater with lower sample coverage and mass. Fe from the Ti metal was removed from the Fe peak areas.

If increasing areal coverage alone accounted for the increase in BT2 signal, we would predict a linear change in the peak areas in proportion to areal coverage. However, features contrary to this prediction are apparent. Relative to lighter elements (energy less than 4 keV), Fe is lower for all samples, indicating that the mean thickness is smaller than the Fe information depth. The relative drop in Fe, evident when normalized to Si (Figure 2b), is lower for the greatest BT2 coverage (78 ± 9%) because the average thickness of the sample was higher due to the piling of grains. The Si/Fe ratio shows the implications for a sample with a mean thickness smaller than the APXS information depth (Figure 3). Variability in Si/Fe as a function of sample thickness shows that deriving element concentrations from a thin sample could be impossible if the thickness is not adequately constrained.

The Na, Mg, and Al signals also drop more than predicted for a reduction in areal coverage (Figure 2). This could arise from two causes: (1) the particulate dusted on the Ti has a different composition than the aliquot used for the bulk

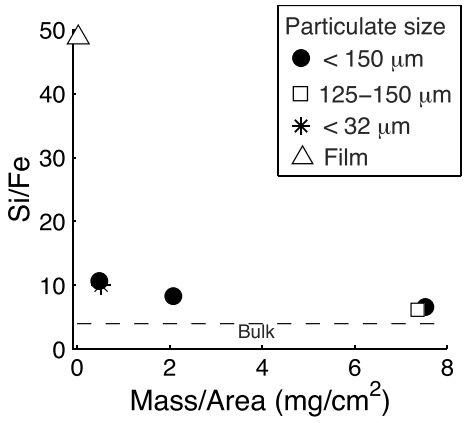

Figure 3. Si/Fe ratios of Ti-tray samples (BT2 + Ti substrate). Si/Fe drops with increasing deposited sample mass because the bigger sample enlarges the depth from which Fe X-rays are excited, whereas the Si X-rays are only seen from the top few micrometers. Therefore, comparison with an infinitely thick sample (BT2 bulk value shown as dashed line) allows us to constrain the mean thickness and mean grain size of sample on the o-tray. Fe from the Ti metal was removed from the Fe peak areas.

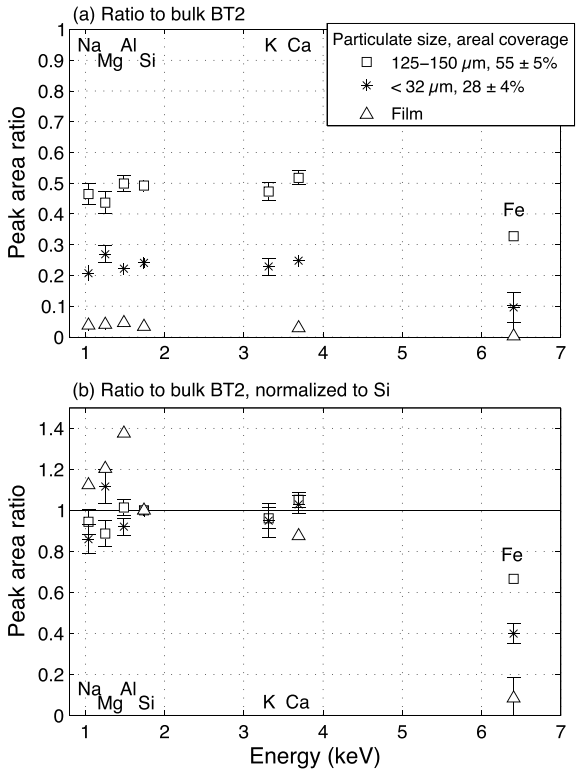

Figure 4. (a) Peak area ratios of various particulate sizes of Ti-tray samples (BT2 + Ti substrate) to the bulk BT2. (b) Peak area ratios normalized to Si. Mineral fractionation caused by sieving is indicated by the Na, Mg, and Al enrichments in the film and the Mg depletion in the largest fraction. Fe from the Ti metal was removed from the Fe peak areas.

measurement and (2) the rough surface of the thin particulate coating caused a drop in signal relative to the pressed, smooth surface of the pellet used for the bulk measurement [*Campbell et al*., 1985]. That Na, Mg, and Al drop the same amount for all three samples (Figure 2b) is evidence that the particulate has the same elemental composition in all Ti-tray samples, and that the dusting process likely did not physically sort the mineral grains, causing compositional changes. This is contradicted by the low K signal in the sample with 12 ± 5% areal coverage; however, K was near the limit of detection (3.7 × limit of detection) and uncertainty is high (20.2%). Nevertheless, the evidence indicates that the three particulates have the same compositions for Ca and lighter elements, thus conclusions can be made about sample coverage and X-ray yield.

Different particulate fractions of BT2 (125–150 μm, < 32 μm, and film) have similar spectral features to those of the < 150 μm fraction, with an increase in BT2 signal proportional to increased areal coverage (Figure 4a). Again due to a thin sample, the Fe signal is lower than the lighter elements. Normalizing to Si highlights differences in the particulate separates (Figure 4b) from the < 150 μm fraction (Figure 2b). In contrast to the < 150 μm fraction, the particulate separates show enrichments in Na, Mg, and Al in the film, and depletions in Mg in the larger fraction. This is evidence of mineral fractionation caused by sieving the BT2 to different particulate sizes than that used for the bulk measurement. Such variation was minimized to within error in the < 150 μm particulate.

4. MSL-APXS O-Tray Measurements

4.1. Sample Acquisition, Dropoff, and APXS Operation

The first solid samples collected by *Curiosity* and delivered to SAM, CheMin, and the o-tray were obtained using the rover's scooping tool during the Rocknest sand shadow sampling campaign (sols 57–100; 3 October to 16 November 2012). The sand shadow was an aeolian sand deposit, inactive and coated with dust that formed in the lee of a cluster of cobbles [*Blake et al*., 2013a]. At the beginning of the sampling campaign, the rover's left front wheel was used to interrogate the material by driving onto the bedform, effectively disturbing it so that its interior could be observed to determine the suitability of the material for scooping and passing through a 150 μm sieve. As shown in Figure 5, five scoops were ultimately

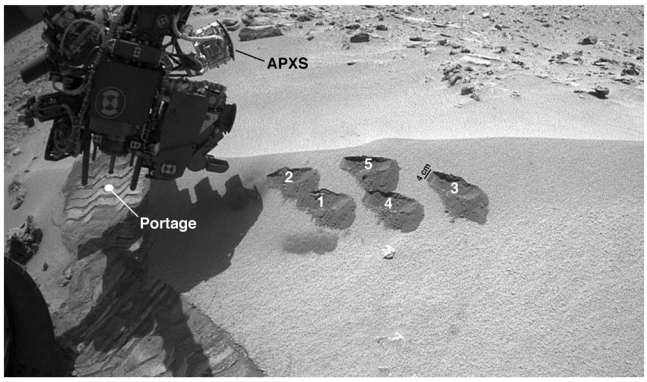

Figure 5. Sol 93 (9 November 2012) Right Hazard Camera A (Hazcam-A) view of the Rocknest sand shadow sampling site after acquisition of the fifth and final scoop. The APXS target inside the scuff created on sol 57 by the left, front wheel is labeled Portage; it was observed by APXS on sol 89. The fifth scoop (labeled 5) was acquired on sol 93; scoop 1 was obtained on sol 61, scoop 2 on sol 66, scoop 3 on sol 69, scoop 4 on sol 74. The APXS instrument head, mounted on the turret at the end of *Curiosity's* robotic arm, is also shown.

collected. The Rocknest sampling campaign and results in detail that are not covered in this work are presented elsewhere [e.g., *Bish et al*., 2013; *Blake et al*., 2013a, 2013b; *Minitti et al*., 2013; *Morris et al*., 2013; *Yen et al*., 2013].

The sampling subsystem on the rover's arm deposits sieved < 150 μm samples on the o-tray using a series of arm and turret movements and mechanical vibrations that move the material into a portioning chamber in CHIMRA [*Anderson et al*., 2012]. CHIMRA is then positioned over the o-tray, the portion chamber is opened, and the sample is dropped on to the o-tray, facilitated by more vibration. Mastcam imaging is used to document the o-tray before and after dropoff. MAHLI images, with working distances ranging about 4–15 cm and corresponding spatial scales of 21–61 μm/pixel, document the sample on the o-tray during the day before nighttime APXS integrations. The APXS instrument is then deployed to the o-tray by the rover's arm, which positions APXS over the sample at a standoff distance deemed safe by the robotic arm operations engineers (0–2 cm). Higher standoff distances may be set to prevent the sample pile from contaminating the instrument. The cooler temperatures of overnight integrations improve spectral resolution, and longer integration times improve counting statistics. Therefore, longer, overnight integrations are best for the small sample volume on the o-tray.

Following an initial sample dropoff test on the o-tray of material from the third scoop on sol 73—in which the sample was observed to have moved out of the tray center (and some moved off the tray)—a series of o-tray dropoff tests were conducted using fourth scoop fines on sol 78. These, too, revealed difficulties in providing the largest possible sample volume within the APXS FOV. Activation of the vibration mechanism in the turret caused the sample deposited on the o-tray to vibrate and move in the direction of the rover's tilt. For the final dropoff of Rocknest fines to the o-tray on sol 95, sieved products from the fifth scoop, vibrations were minimized. However, much of the samples moved away from the center of the o-tray, some of it out of the APXS FOV.

The sols 73 and 78 dropoff tests also confirmed that the o-tray had a layer of dust, evident in the first MAHLI image of the tray, acquired on sol 37, and rendered more obvious and apparent when the sample movement cleared off dust as it vibrated off the tray. As with other rover surfaces, the dust was initially deposited during landing, with additions likely coming from dust settling from the atmosphere and possibly lofted by the rover wheels on sols thereafter. For this reason, an APXS measurement of the "empty" o-tray was conducted before the measurement of the Rocknest fines to investigate the dust layer. Empty indicates an o-tray measurement without a scooped or drilled sample and does not imply a clean surface.

Table 4. MSL-APXS O-Tray Target Summary

Target	Sol	Integration Time (s)	FWHM Mn (eV)[a]	Instrument Standoff (cm)	Description
Portage	89	9,303	138.8	2	Rocknest fines in situ
Empty_otray	91	17,178	149.9	0	O-tray with dust, some Rocknest material
RN_soil_otray	95	17,247	142.1	2	O-tray with scooped and sieved Rocknest sample
Empty_otray	177	8,898	158.9	0	O-tray with dust

[a]FWHM, Full width at half maximum.

Table 5. MSL-APXS Peak Areas of O-Tray and Rocknest Measurements[a]

	Empty_otray sol 91		Empty_otray sol 177		Portage sol 89 In Situ Fines		RN_fines_otray sol 95 Sample on O-Tray	
Sample	Area (cts/s)	%Fit Error	Area (cts/s)	%Fit Error	Area (cts/s)	%Fit Error	Area (cts/s)	%Fit Error
Na	0.42	16.2	0.85	12.8	2.75	8.3	0.84	12.8
Mg	1.72	6.7	3.31	6.0	12.3	4.4	4.07	5.2
Al	3.69	4.7	5.22	5.4	20.1	4.0	6.62	4.6
Si	9.72	2.3	17.0	2.1	80.4	2.0	25.4	2.2
S	0.79	8.1	1.55	6.9	4.61	4.6	1.71	5.9
Cl	0.19	30.2	0.35	24.9	1.09	9.5	0.38	17.8
K	nd		nd		0.82	10.3	0.26	21.2
Ca	0.87	8.7	1.13	9.1	7.24	3.2	2.13	5.3
Ti	237.3	1.2	233.1	1.3	1.07	7.5	106.4	1.5
Mn	nd		nd		0.85	11.1	0.15	22.7
Fe	3.14	2.3	2.20	3.3	52.7	1.7	10.3	2.1
Ni	0.04	42.2	0.04	56.2	0.19	21.6	0.05	51.4
Zn	0.03	52.5	nd		0.27	15.9	0.07	37.1

[a]Peak areas are scaled to represent the same standard geometry with geometric normalization = 1. The geometric normalization of the empty o-tray measurements is 1.00. For Portage sol 89 and RN_fines_otray sol 95 the geometric normalization is 0.33 ± 0.05, and Na, Mg, Al, and Si peak areas are increased by 10%, 6%, 4%, and 2%, respectively, to account for attenuation in the longer column of 8.1 mBar CO_2 between the sample and detector. nd = not detected.

The primary purpose of the o-tray is to enable APXS measurements of samples processed for delivery to SAM and ChemMin. This is important to identify differences in the sample relative to the in situ measurements. To do this, we evaluate the o-tray measurements relative to the in situ target "Portage," an APXS measurement of Rocknest fines on sol 89 [*Yen et al.*, 2013]. It is important to mention that Portage was measured on the floor of a wheel scuff (so the loose material would be compressed for safe contact with the APXS contact sensor), while the fifth scoop was done in a different area of the Rocknest bedform (Figure 5). A summary of MSL-APXS measurements relevant to the o-tray is presented in Table 4.

4.2. MSL-APXS O-Tray Results

4.2.1. Empty O-Tray

APXS measurements of the empty o-tray were conducted on sols 91 and 177, bracketing the Rocknest sample measurement on sol 95 (Table 5). The first empty o-tray measurement on sol 91 contained remnants of Rocknest sample portions deposited on the o-tray for testing purposes, evident as larger grains (Figure 6a). Fine, red dust previously coated the o-tray but was partially cleaned off by the vibration of test portions on the o-tray before the sol 91 APXS measurement. Before the sol 177 APXS measurement of the empty o-tray (Figure 6b), the Rocknest sample had vibrated completely off of the o-tray due to turret vibrations and rover driving. More dust appears to have been redeposited on the o-tray. The removal of Rocknest sample and deposition of dust occurred over sols 100–177. Both empty o-tray spectra were acquired with the instrument's contact sensor touching the tray; these results show sizeable Ti K peaks, Ti background, and Ti escape peak

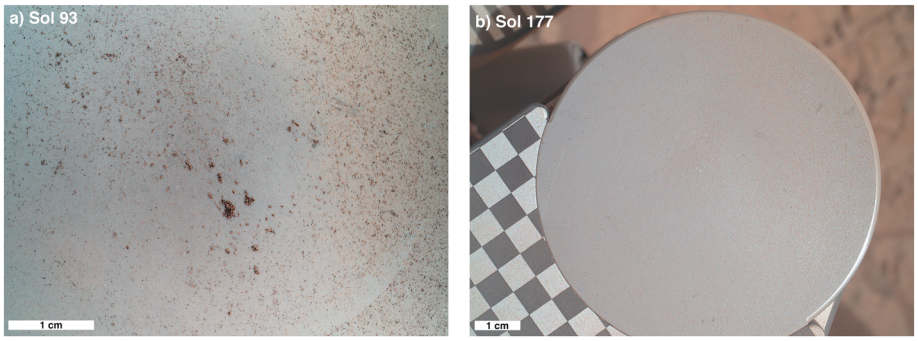

Figure 6. MAHLI images documenting two APXS measurements of the empty o-tray on *Curiosity*. (a) The empty o-tray on sol 93, documenting the state after the sol 91 APXS measurement, with some Rocknest scoop 4 sand grains remaining after sample dropoff tests. The red hue in the right of the image is fine dust. (b) Dust on the o-tray before the sol 177 measurement of the empty o-tray.

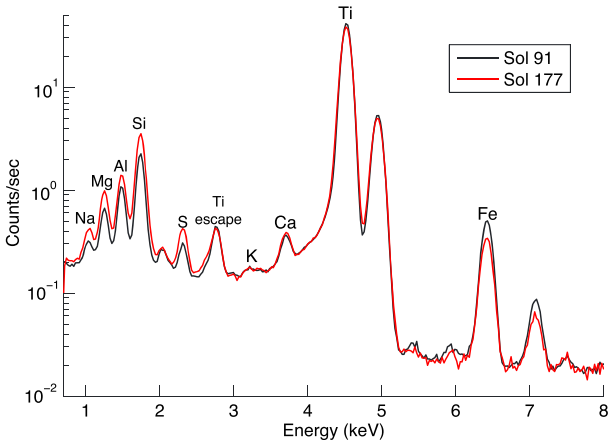

Figure 7. MSL-APXS spectra of the empty o-tray on sols 91 and 177. Contribution from the dust is apparent in peaks not associated with the Ti metal (e.g., Na, Mg, and Al). Select Kα peaks and the Ti Kα escape peak are labeled.

(Figure 7). The presence of material on the o-tray is clear from the intensity of other peaks not observed in the APXS spectrum of the clean Ti metal (cf. Figure 1).

Comparison of the peak area ratios of the empty o-trays to the Rocknest bulk target Portage reveals differences between the two measurements (Figure 8). Note that the empty o-tray spectra were taken in contact, while Portage was measured with 2 cm standoff for safe deployment. To account for this standoff difference, a geometric normalization factor of 0.33 ± 0.05 was applied to the peak areas of the empty o-tray spectra. Additional corrections were made to Na, Mg, Al, and Si for Portage (increases of 10%, 6%, 4%, and 2%, respectively) to account for attenuation in the longer column of 8.1 mBar CO_2 between the sample and detector. On sol 91, all elements lighter than Ti were lower than on sol 177, while Fe was higher. Smaller differences between the two measurements could be attributed to compositional differences; however, the broader trend may be explained by the state of the material on the o-tray (see section 5.3).

4.2.2. Rocknest Sample

Martian regolith fines deposited in the Rocknest sand shadow were investigated by APXS in situ at the target Portage on sol 89 and on the o-tray on sol 95. The in situ target was within *Curiosity's* wheel track, which disturbed the aeolian structure of the Rocknest sand shadow [*Blake et al*., 2013b] (Figure 5). As observed in MAHLI images acquired just before APXS placement, grains within the APXS FOV are bimodal, consisting of (1) rounded to subrounded, mm-sized grains with colors ranging from clear to brown/red to black and (2) fine sand and smaller grains (Figure 9) [*Minitti et al*., 2013]. The mm-sized grains are likely derived from the armor on the surface of the sand shadow, mixed in with the finer underlying material by the rover's wheel. When APXS was deployed, the contact plate touched the surface, and then backed off to integrate at a standoff distance of 2 cm. The Portage spectrum is typical of mafic (also known as "basaltic") rocks and fines (Figure 10); the composition is similar to regolith fines and aeolian bedforms observed at the two Mars Exploration Rover sites [*Blake et al*., 2013a; *Gellert et al*., 2013; *Yen et al*., 2013].

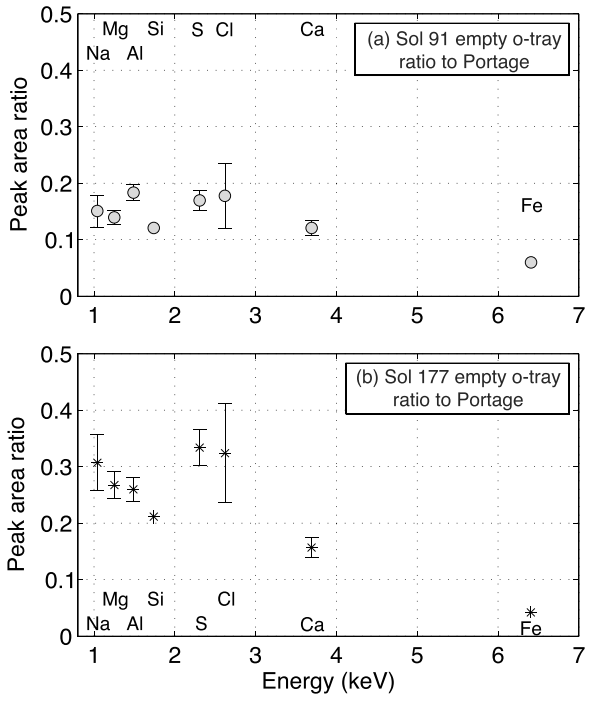

Figure 8. Peak area ratios of empty o-tray measurements on (a) sol 91 and (b) sol 177 to the in situ fines at the target named Portage. Potassium and Mn are near detection limits and are not shown.

On sol 95, scooped and sieved (<150 μm) fines from Rocknest were analyzed by APXS on the o-tray with 2 cm standoff. MAHLI images show a range of particle types indicative of a variety of crystalline mineral grains, lithic fragments, dust and dust aggregates, and other grains [*Minitti et al*., 2013; *Blake et al*., 2013b; *Edgett et al*., 2013] (Figure 11). Based on the color contrast

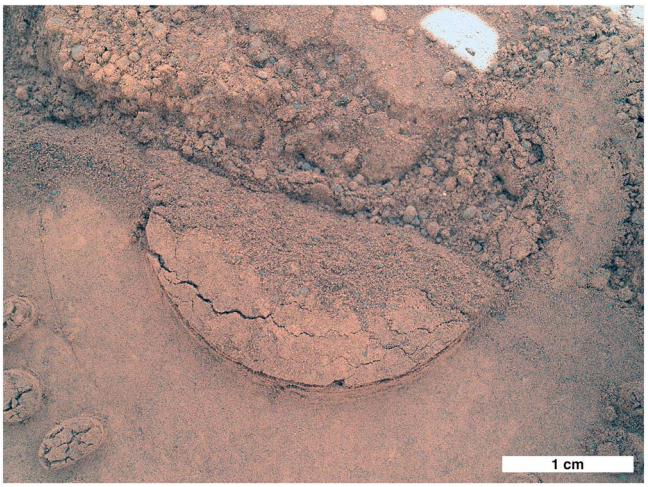

Figure 9. MAHLI image of the APXS target Portage in the Rocknest sand shadow (sol 89). The circular form centered in the middle of the image is the imprint of the APXS contact plate in the sand. The APXS FOV is ~3.1 cm in diameter, centered in the middle of the image.

between the sample and Ti o-tray in MAHLI microscopic images, we determined the sample areal coverage to be 30 ± 5% of the ~3.1 cm FOV. Although highly variable in vertical distribution, we estimate from the MAHLI images a maximum sample thickness of ~0.5–1.2 mm. The minimum thickness is not resolvable at 32 μm per pixel. Some of the samples moved out of the APXS FOV when the sampling subsystem caused vibration of the o-tray. The spectrum of the sample on the o-tray exhibits a prominent Ti peak and elevated background over the lower energy portion of the spectrum < 5 keV (Figure 10).

The peak areas of the sample on the o-tray are directly comparable to those of the in situ target, Portage, because standoff distances were the same (Table 5; Figure 12). Peak area ratios are ~1/3 across the spectrum relative to the bulk sample, suggesting that ~1/3 of the APXS FOV contains sample. This is consistent with the 30 ± 5% areal coverage observed in MAHLI images. On the o-tray, the Ca, Mn, and Fe signals drop with increasing *Z*, indicating that a fraction of the sample is thinner than the typical APXS sampling depth for the heavier elements [*Rieder et al*., 2003; *Brückner et al*., 2008]. Slightly elevated S and Cl (however, within the error bars), with a S/Cl ratio similar to that found by the Mars Exploration Rovers (MER) [*Gellert et al*., 2006], could indicate a small enrichment of these two elements in the < 150 μm portion delivered to the o-tray. However, variation of S and Cl in parallel was found in regolith fines observed at the MER sites, so the o-tray sample would fit within the typical range of S and Cl contents found in MER basaltic regolith fines [*Yen et al*., 2005, 2013].

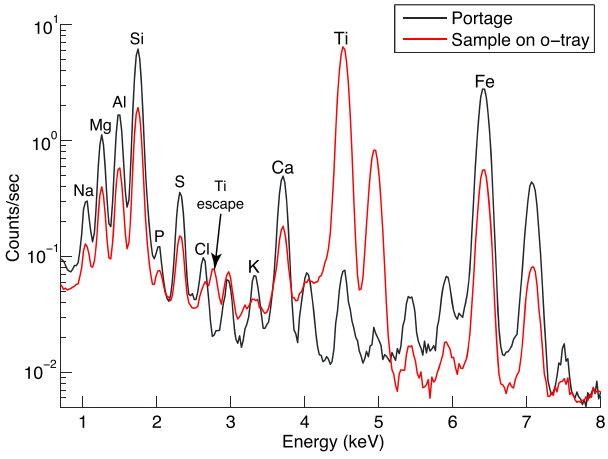

Figure 10. MSL APXS spectra of Rocknest fines in situ (Portage; sol 89) and on the o-tray (sol 95). The spectrum of the sample on the o-tray exhibits a prominent Ti peak and elevated background over < 5 keV. Select Kα peaks and the Ti Kα escape peak are labeled.

5. Discussion

As demonstrated above, thin coatings of particulate samples present challenges to derivation of chemical concentrations from APXS spectra. However, we do observe relationships that constrain the properties of samples on a Ti substrate. Three components must be taken into account to evaluate an o-tray sample, relative to the bulk: (1) partial areal coverage, (2) the thin layer effect, and (3) compositional fractionation. Areal

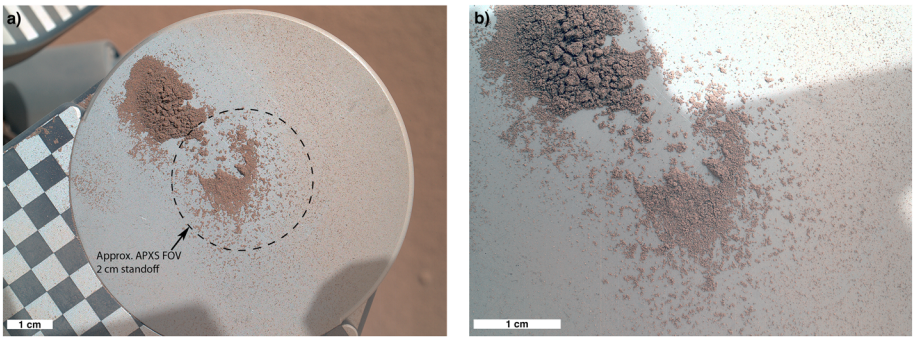

Figure 11. MAHLI images of the Rocknest fifth scooped and sieved sample on the o-tray on sol 95. The sample moved partially out of the APXS field of view (~3.1 cm in diameter centered in the image) due to vibration by the sampling subsystem.

coverage can be estimated from images, by the proportional drop in intensity across the spectrum (Figures 2 and 4), and by the attenuation of Ti due to sample obscuring the tray (section 5.2.). The thin layer effect is well understood and may be predicted (section 5.1). If systematic spectral changes due to partial areal coverage and the thin layer effect can be isolated, it might be possible to determine practical corrections and identify compositional fractionation, a possibility we discuss below.

5.1. Modeling X-Ray Yields for Thin Samples

To better understand the properties of the Ti-tray and o-tray samples, we have used a new computer code APXyield. This program calculates the yield of characteristic X-rays for thin and layered samples with known compositions using fundamental PIXE and XRF principles. Homogeneous, continuous, and flat layers are assumed. This is an appropriate assumption for the Ti metal substrate; however, particulates on Ti metal may not fit this assumption well. Nevertheless, we find this model to be informative. Figure 13 shows how low *Z* elements below ~ Ca reach 90% of a bulk sample signal at thicknesses less than 10 μm, while higher *Z* elements like Fe need thicker layers to deliver a full bulk signal. Also notable is the excitation of Ca, K, and Cl by X-rays from the Ti substrate, resulting in X-ray yields higher than in the bulk sample. In the following discussion, we compare the X-ray yield model to our observations of the Ti-tray and o-tray samples and consider the possibility of using it to apply corrections to APXS data.

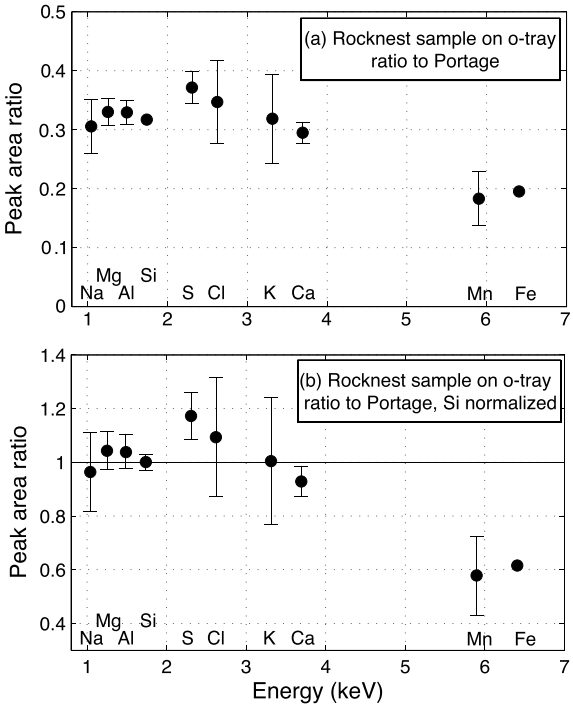

Figure 12. (a) Peak area ratios of Rocknest sample on the o-tray to the in situ Portage fines. Peak area ratios are ~1/3 across the spectrum relative to the bulk sample, suggesting that ~1/3 of the APXS FOV contains sample. (b) Peak area ratios normalized to Si. The Ca, Mn, and Fe signals drop with increasing *Z*, indicating that a fraction of the sample is thinner than the APXS sampling depth. Elevated S and Cl indicate a small enrichment of these two elements.

The Ti-tray and o-tray data show that Fe is the major element most affected by the thin layer effect, so our approach focuses on iron. The X-ray yield of a sample that only partially covers the substrate cannot be directly compared to a model that assumes 100% coverage without applying a correction for areal coverage. We assume the signal from the thin sample increases linearly in proportion to areal coverage (see section 5.2.) and divide the Fe peak area by the fraction of areal coverage. Having applied this correction, we can use the comparison of the Fe signals of Ti-tray and bulk to extract the mean thickness. Note that this

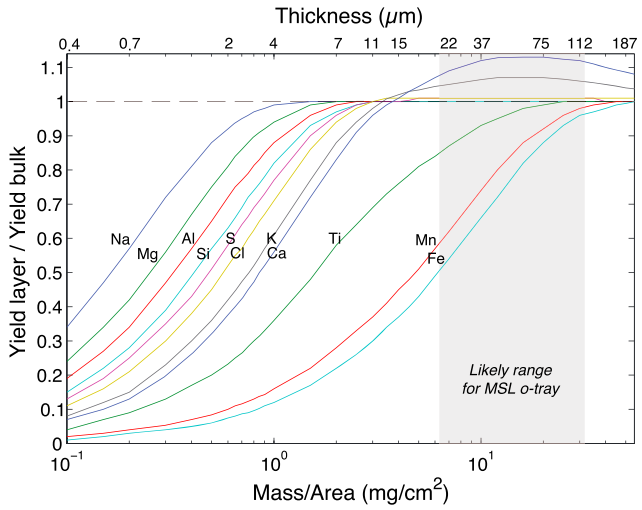

Figure 13. Modeled APXS X-ray yield curves (from APXyield) for a layer of Martian regolith fines composition (MSL APXS, Portage) on a Ti substrate. The model shows the drop in yield from a thin layer relative to the bulk yield. The gray field indicates a range of mass/area values likely for portions delivered by the MSL sampling subsystem to the o-tray. Cl, K, and Ca yields are greater than the bulk due to the flux of Ti X-rays from the o-tray. Thickness values are calculated assuming a sample density of 2.67 g/cm^3.

model assumes that the sample is homogeneous, i.e., Si and Fe and all other elements are in the same homogeneous grains. The correction for areal coverage is also carried out on the measured mass per unit area value to enable a consistent comparison of mean thickness and Fe signals. When corrected for areal coverage, the Ti-tray data follow the APXyield modeled increase in Fe signal with increasing sample mass/area (Figure 14). The mass/area spread of the data, however, is not adequate for evaluating most of the modeled curve. In addition, this data set is not sufficient to thoroughly test the assumption of a homogeneous, uniformly thick layer. Others have discussed the implications of heterogeneity in natural samples [e.g., *Campbell et al*., 2012], but the variable thickness of particulate samples is likely more of a challenge to the model's assumptions. Supposing the modeled yield represents a mean thickness, and the model is accurate over a larger mass/area range, it is useful for understanding the properties of o-tray samples.

For samples investigated by *Curiosity*, we must assume either (1) a mean sample thickness or (2) the Fe content of the o-tray sample is equal to the bulk. Using APXyield, we can model the expected signal for any layer thickness. If the thickness is known, then deviation from the model indicates enrichment or depletion in the o-tray sample relative to the bulk. If the Fe content is assumed to be the same in the o-tray sample and the bulk, then the mean sample thickness can be determined. It is important to note that the signal dropoff for thin layers has a well-defined and smooth behavior with increasing *Z*. This can be used to first check the assumption of a thin layer. Then, we look for statistically significant deviations from the expected drop in signal. These deviations must stem from a difference in absolute abundance and can be quantified relative to the bulk abundance. If the sample thickness is not known, then it is not possible to uniquely identify element enrichment/depletion from the drop in element signal due to a thin sample. Such is the case for the sol 95 measurement of Rocknest fines on the o-tray, which had highly variable and poorly constrained thickness. With this approach, we are not able to uniquely identify differences in Mn and Fe content between the in situ Rocknest target (Portage) and Rocknest fines processed by CHIMRA and dropped on the o-tray (Figure 12b).

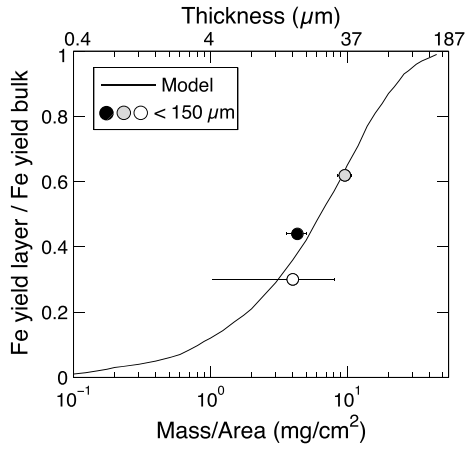

Figure 14. Modeled Fe X-ray yield (from APXyield) for thin BT2 layers compared with the measured Fe yield for the $<$ 150 μm Ti-tray samples, shown as a ratio to bulk BT2. The Fe yield and mass/area of the BT2 samples are corrected for partial areal coverage (see text). Thickness is derived from mass/area, assuming a density of 2.67 g/cm^3. Fe from the Ti metal was removed from the Fe peak areas.

5.2. Spectral Contributions From the Ti Substrate

The decrease in Ti peak area with increasing sample coverage may be used to constrain the overall portion size. Increasing the areal coverage of the sample lowers the Ti signal systematically (Figure 15a). However, this is not expected to be linear for thin samples ($<$ 30 μm) that allow

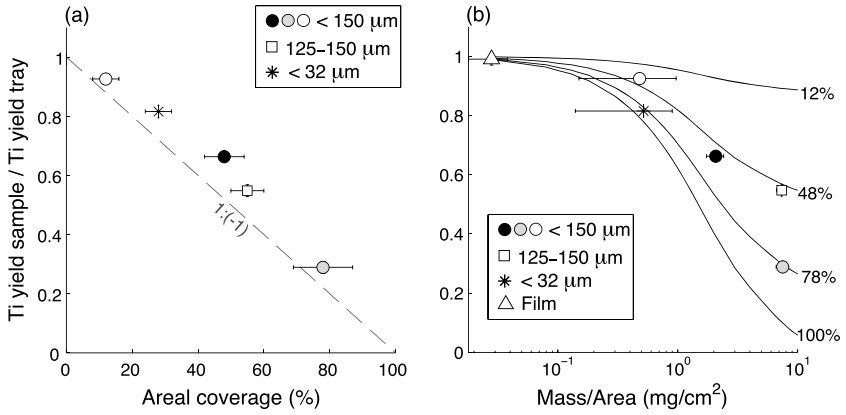

Figure 15. Decrease of Ti yield due to increasing sample coverage for the Ti-tray samples as a function of (a) % areal coverage and (b) mass/area. The modeled yield (from APXyield) for a Ti substrate with a thin BT2 sample is shown in Figure 15b (solid lines). The model shows the difference in response for 12%, 48%, 78%, and 100% areal coverage of the sample layer. Particulate size is denoted in the legends.

partial transmission of Ti X-rays from the substrate through the sample. Transmission of Ti through the BT2 layer is a likely reason the Ti-tray sample data plot over the 1:−1 line in Figure 15a; contribution of Ti counts from the sample is less than 1% of the total signal. To evaluate the effect of areal coverage, we modeled the X-ray yield (with APXyield) of Ti metal with a BT2 layer having a range of mass/area values (Figure 15b). To model the APXS response with different areal coverage amounts, we assume the Ti signal from the exposed substrate mixes linearly with the attenuated Ti signal from the coated substrate in proportion to areal coverage of the BT2 layer. The *y* axis in Figure 15b shows the ratio (coated sample Ti yield)/(uncoated metal Ti yield) at areal coverage of 100%, 78%, 48%, and 12%, the latter three being the areal coverage of the < 150 μm Ti-tray samples. The Ti-tray samples with mass/area > 1 fit well with the modeled yield; smaller samples had error too large to compare. The sample set is too small to make quantitative conclusions about the accuracy of the modeling.

These laboratory observations of Ti attenuation might be useful for estimating sample coverage on the MSL o-tray. However, dust on the o-tray prevents an MSL-APXS measurement of a dust-free, clean o-tray for comparison with the o-tray containing a sample. Further work to characterize the dusty empty o-tray is ongoing. For this reason, MAHLI images of the sample on the o-tray are critical to estimating sample size.

Iron in the Ti metal is at a concentration above APXS detection limits. The potential skew of iron concentrations due to Fe in the Ti metal can be estimated by the metal's Fe peak relative to those of the Ti-tray samples (Figure 16). While the Ti metal may add a measureable number of Fe counts if the sample volume is small, because of the uncertainty in concentration due to the thin layer effect, this number is most likely within error. If, however, a study of dust films on the o-tray is conducted, Fe in the metal will likely add a significant number of counts.

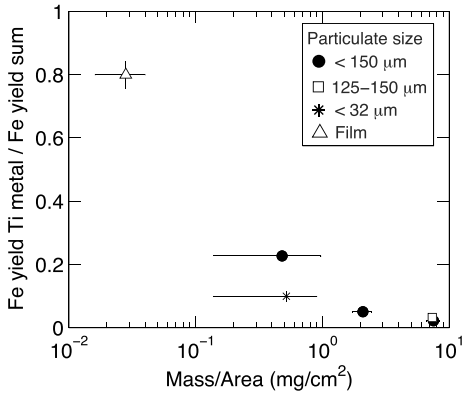

Figure 16. X-ray yield from Fe impurity in the Ti metal substrate as a fraction of total Fe yield for the Ti-tray samples (BT2 + Ti substrate).

An increased background < 5 keV contributed by the Ti substrate adds error to APXS spectrum fitting. Smaller amounts of material on the Ti-tray reduce X-ray counts, increasing the error (Table 3). Unsurprisingly, this effect is greater for elements with a lower abundance in the bulk material, such as K and Mn in BT2 basalt.

5.3. Empty O-Tray and Dust

APXS measurements of the empty o-tray are useful for identifying possible background contributions to samples on the o-tray and might be important for understanding the dust environment around *Curiosity*. The two empty o-tray measurements on sols 91 and 177 have key differences

(Figure 8). Small differences between the two empty o-tray measurements may be attributable to composition. However, the large relative discrepancies are more plausibly due to the physical arrangement of the material on the o-tray. As evident from MAHLI images acquired on sols 85 and 93 (Figure 6), the APXS FOV on sol 91 contained a mixture of sand-sized Rocknest grains, patchy dust, and patches of clean titanium. This is similar to the Ti-tray experiments described above, and the resulting plots of peak area ratios are relatively flat at a value proportional to areal coverage and dropoff with increasing Z (Figures 2, 4, and 12). In contrast, on sol 177, the o-tray had only a layer of dust that is likely very fine-grained, with particle sizes ~1–2 μm found in past studies [e.g., *Pollack et al*., 1995; *Tomasko et al*., 1999; *Clancy et al*., 2003]. For a thin, continuous layer a few micrometers thick, a predicted plot of peak area ratios would decrease regularly with increasing Z as the thin layer effect results in a progressively greater drop in signal. We observe this trend in the sol 177 data with the notable exception of S and Cl enrichments (Figure 8). This result is in agreement with previous observations of dust on the MER missions. The airborne dust is fine, brighter in images, and enriched in S and Cl, likely bound in a ferric iron phase [*Yen et al*., 2005; *Morris et al*., 2006].

An alternative explanation for smaller peak areas of lighter elements on sol 91 could be that there was a larger volume of material on the o-tray on sol 177 than on sol 91. This is unlikely because Fe would be lower on sol 91 as well; instead it is ~1.5 higher on sol 91. The key to the difference is the exposed, clean Ti surface, which causes the overall drop in signal of the lighter elements.

Under some circumstances, the presence of dust on the o-tray may skew results for samples on the o-tray. The results from the sol 177 empty o-tray show that the presence of a thin dust film can yield counts for Na, Mg, Al, and Si that are 20–30% of a bulk measurement. This could be minimized by increasing the amount of sample in the FOV or by cleaning the o-tray with the rover's Dust Removal Tool (DRT), though the latter has not yet been attempted and could introduce its own complications (e.g., the DRT may scratch the o-tray, potentially trapping fines in grooves).

5.4. APXS Strategy for MSL O-Tray

As outlined in this work, variability and uncertainty are expected for any APXS measurement of material on *Curiosity's* o-tray. Despite these limitations, the APXS observations of samples deposited on the o-tray are vital to characterizing the samples analyzed by SAM and CheMin. We emphasize that o-tray measurements are most valuable as a comparison to bulk sample APXS analyses, where the high precision allows for determination of differences in certain elements. Bulk measurements should take priority over o-tray measurements if rover resources are limited. We recommend the following strategies to maximize the scientific return from o-tray measurements with APXS:

1. Deposit multiple portions on the o-tray to maximize the amount of material within the APXS FOV.
2. Improve targeting of the sample pile placement on the o-tray for a given rover tilt to maximize the sample amount.
3. Measure unused sample after the CHIMRA deposits it on the ground to obtain bulk sample spectra.
4. Periodically measure air-fall dust that has accumulated on the o-tray.

6. Final Remarks

The purpose of this study was to develop a practical method for interpreting APXS measurements of the o-tray and material on the o-tray, so that the APXS can be used to characterize portions of the same samples that are delivered to SAM and CheMin. Our results show that the APXS response for thin, particulate samples on a Ti substrate is predictable with respect to areal coverage and sample thickness, therefore, differences in composition relative to the bulk can be identified. We find a slight enrichment of S and Cl in the sol 95 o-tray Rocknest sample, an aliquot of the scooped and sieved material delivered to SAM and CheMin. We find no evidence that the composition is otherwise different than the Rocknest sand target named Portage. Exceptions are Mn and Fe, for which the thin layer effect caused a drop in signal that cannot be uniquely distinguished from differences in concentration between the o-tray sample and Portage. Knowing the mean sample thickness on the o-tray would enable a correction for the thin layer effect. However, given the large uncertainties involved, we do not find it useful to derive APXS oxide concentrations for the Rocknest sample measured on the o-tray.

Acknowledgments
The MSL-APXS was managed and financed by the Canadian Space Agency (CSA), with MDA as prime contractor to build the instrument. Science team funding is provided by CSA and NASA/JPL-Caltech. We appreciate and acknowledge the unwavering support of dedicated engineers at MDA, CSA, and JPL during the development and operation. P.L. King was supported by contracts from CSA, NASA/JPL-Caltech, and a New Mexico Experimental Program to Stimulate Competitive Research grant that funded J.A. Berger, who was also supported by the Institute of Meteoritics, University of New Mexico, Albuquerque, NM. K.S. Edgett's contribution, via the MSL MAHLI investigation, was performed under NASA/JPL-Caltech contract 1273887.

References

Anderson, R. C., et al. (2012), Collecting samples in Gale Crater, Mars; an overview of the Mars Science Laboratory sample acquisition, sample processing and handling system, *Space Sci. Rev.*, *170*(1–4), 57–75, doi:10.1007/s11214-012-9898-9.

Bell, J. F., M. C. Malin, M. A. Caplinger, M. A. Ravine, A. S. Godber, M. C. Jungers, M. S. Rice, and R. B. Anderson (2012), Mastcam multispectral imaging on the Mars Science Laboratory Rover: Wavelength coverage and imaging strategies at the Gale Crater field site, presented at Lunar Planet. Sci. Conf., XLIII, Abstract 2541.

Bish, D. L., et al. (2013), X-ray diffraction results from Mars Science Laboratory: Mineralogy of Rocknest at Gale Crater, *Science*, *341*(6153), 1238932, doi:10.1126/science.1238932.

Blake, D., et al. (2012), Characterization and calibration of the CheMin Mineralogical Instrument on Mars Science Laboratory, *Space Sci. Rev.*, *170*(1–4), 341–399, doi:10.1007/s11214-012-9905-1.

Blake, D. F., et al. (2013a), Curiosity at Gale Crater, Mars: Characterization and analysis of the Rocknest sand shadow, *Science*, *341*(6153), 1239505, doi:10.1126/science.1239505.

Blake, D. F., et al. (2013b), Mineralogy and elemental composition of wind drift soil at Rocknest, Gale crater, presented at Lunar Planet. Sci. Conf., XLIV, Abstract 1289.

Brückner, J., G. Dreibus, R. Gellert, S. W. Squyres, H. Wänke, A. Yen, and J. Zipfel (2008), Mars Exploration Rovers: Chemical composition by the APXS, in *The Martian Surface*, vol. 1, edited by J. F. Bell III, pp. 58–101, Cambridge Univ. Press, New York.

Burkemper, L., P. L. King, R. Gellert, M. N. Spilde, and R. M. Chamberlin (2008), Characterization of the basalt of Broken Tank, NM for the "in situ" calibration target for the Alpha-Particle X-ray Spectrometer (APXS) on the upcoming Mars Science Laboratory (MSL) Rover, Abstracts 1464 presented at 2008 Fall Meeting, AGU San Francisco, Calif., 15–19 Dec.

Campbell, J. L., and J. A. Cookson (1984), PIXE analysis of thick targets, *Nucl. Instrum. Methods Phys. Res., Sect. B*, *3*(1–3), 185–197, doi:10.1016/0168-583X(84)90361-6.

Campbell, J. L., R. D. Lamb, R. G. Leigh, B. G. Nickel, and J. A. Cookson (1985), Effects of random surface roughness in PIXE analysis of thick targets, *Nucl. Instrum. Methods Phys. Res., Sect. B*, *12*(3), 402–412, doi:10.1016/0168-583X(85)90040-0.

Campbell, J. L., M. Lee, B. N. Jones, S. M. Andrushenko, N. G. Holmes, J. A. Maxwell, and S. M. Taylor (2009), A fundamental parameters approach to calibration of the Mars Exploration Rover Alpha Particle X-ray Spectrometer, *J. Geophys. Res.*, *114*, E04006, doi:10.1029/2008JE003272.

Campbell, J. L., S. M. Andrushenko, S. M. Taylor, and J. A. Maxwell (2010), A fundamental parameters approach to calibration of the Mars Exploration Rover Alpha Particle X-ray Spectrometer: 2. Analysis of unknown samples, *J. Geophys. Res.*, *115*, E04009, doi:10.1029/2009JE003481.

Campbell, J. L., J. A. Maxwell, S. M. Andrushenko, S. M. Taylor, B. N. Jones, and W. Brown-Bury (2011a), A GUPIX-based approach to interpreting the PIXE-plus-XRF spectra from the Mars Exploration Rovers: I. Homogeneous standards, *Nucl. Instrum. Methods Phys. Res., Sect. B*, *269*(1), 57–68, doi:10.1016/j.nimb.2010.10.004.

Campbell, J. L., A. M. McDonald, G. M. Perrett, and S. M. Taylor (2011b), A GUPIX-based approach to interpreting the PIXE-plus-XRF spectra from the Mars Exploration Rovers: II Geochemical reference materials, *Nucl. Instrum. Methods Phys. Res., Sect. B*, *269*(1), 69–81, doi:10.1016/j.nimb.2010.09.014.

Campbell, J. L., G. M. Perrett, R. Gellert, S. M. Andrushenko, N. I. Boyd, J. A. Maxwell, P. L. King, and C. D. M. Schofield (2012), Calibration of the Mars Science Laboratory Alpha Particle X-ray Spectrometer, *Space Sci. Rev.*, *170*(1–4), 319–340, doi:10.1007/s11214-012-9873-5.

Campbell, J. L., J. A. Berger, R. Gellert, P. L. King, G. M. Perrett, N. I. Boyd, K. S. Edgett, R. A. Yingst, and M. S. L. Science Team (2013), First measurements of the MSL APXS calibration target on Mars, presented at Lunar Planet. Sci. Conf., XLIV, Abstract 1506.

Clancy, R. T., M. J. Wolff, and P. R. Christensen (2003), Mars aerosol studies with the MGS TES emission phase function observations: Optical depths, particle sizes, and ice cloud types versus latitude and solar longitude, *J. Geophys. Res.*, *108*(E9), 5098, doi:10.1029/2003JE002058.

Edgett, K. S., et al. (2012), Curiosity's Mars Hand Lens Imager (MAHLI) investigation, *Space Sci. Rev.*, *170*(1–4), 259–317, doi:10.1007/s11214-012-9910-4.

Edgett, K. S., et al. (2013), Mars Hand Lens Imager (MAHLI) efforts and observations at the "Rocknest" eolian sand shadow in Curiosity's Gale Crater field site, presented at Lunar Planet. Sci. Conf., XLIV, Abstract 1201.

Foley, C. N., T. E. Economou, R. N. Clayton, J. Brückner, G. Dreibus, R. Rieder, and H. Wänke (2008), Martian surface chemistry: APXS results from the Pathfinder landing site, in *The Martian Surface*, vol. 1, edited by J. F. Bell III, pp. 35–57, Cambridge Univ. Press, New York.

Gellert, R., et al. (2006), Alpha Particle X-Ray Spectrometer (APXS): Results from Gusev crater and calibration report, *J. Geophys. Res.*, *111*, E02S05, doi:10.1029/2005JE002555.

Gellert, R., J. L. Campbell, P. L. King, L. A. Leshin, G. W. Lugmair, J. G. Spray, S. W. Squyres, and A. S. Yen (2009), The Alpha-Particle-X-Ray-Spectrometer (APXS) for the Mars Science Laboratory (MSL) Rover Mission, presented at Lunar Planet. Sci. Conf., XL, Abstract 2364.

Gellert, R., et al. (2013), Initial MSL APXS activities and observations at Gale Crater, Mars, presented at Lunar Planet. Sci. Conf., XLIV, Abstract 1432.

King, P. L., et al. (2010), Extended calibrations for the APXS for the Mars Science Laboratory mission, presented at Lunar Planet. Sci. Conf., XLI, Abstract 2539.

Mahaffy, P., et al. (2012), The sample analysis at Mars investigation and instrument suite, *Space Sci. Rev.*, *170*(1–4), 401–478, doi:10.1007/s11214-012-9879-z.

Minitti, M. E., et al. (2013), MAHLI at the Rocknest sand shadow: Science and science-enabling activities, *J. Geophys. Res. Planets*, *118*, 2338–2360, doi:10.1002/2013JE004426.

Morris, R. V., et al. (2006), Mössbauer mineralogy of rock, soil, and dust at Meridiani Planum, Mars: Opportunity' journey across sulfate-rich outcrop, basaltic sand and dust, and hematite lag deposits, *J. Geophys. Res.*, *111*, E12S15, doi:10.1029/2006JE002791.

Morris, R. V., et al. (2013), The amorphous component in Martian basaltic soil in global perspective from MSL and MER missions, presented at Lunar Planet. Sci. Conf., XLIV, Abstract 1653.

Omand, M., J. L. Campbell, and J. A. Maxwell (2005), Simulation of the relationship between element concentrations and X-ray yields in the Mars Exploration Rover's X-ray spectrometer, *Nucl. Instrum. Methods Phys. Res., Sect. B*, *229*(1), 123–136, doi:10.1016/j.nimb.2004.11.014.

Pollack, J. B., M. E. Ockert-Bell, and M. K. Shepard (1995), Viking Lander image analysis of Martian atmospheric dust, *J. Geophys. Res.*, *100*(E3), 5235–5250, doi:10.1029/94JE02640.

Rieder, R., R. Gellert, J. Brückner, G. Klingelhöfer, G. Dreibus, A. Yen, and S. W. Squyres (2003), The new Athena alpha particle X-ray spectrometer for the Mars Exploration Rovers, *J. Geophys. Res.*, *108*(E12), 8066, doi:10.1029/2003JE002150.

Thompson, L. M., et al. (2013), BT2 calibration target for Mars Science Laboratory Alpha Particle X-ray Spectrometer: Characterization and alkali basalt Martian analogue, presented at Lunar Planet. Sci. Conf., XLIV, Abstract 2190.

Tomasko, M. G., L. R. Doose, M. Lemmon, P. H. Smith, and E. Wegryn (1999), Properties of dust in the Martian atmosphere from the Imager on Mars Pathfinder, *J. Geophys. Res.*, *104*(E4), 8987–9007, doi:10.1029/1998JE900016.

Yen, A. S., et al. (2005), An integrated view of the chemistry and mineralogy of Martian soils, *Nature*, *436*(7047), 49–54, doi:10.1038/nature03637.

Yen, A. S., et al. (2013), Evidence for a global Martian soil composition extends to Gale Crater, presented at Lunar Planet. Sci. Conf., XLIV, Abstract 2495.